WAKE ROLL-UP BEHIND WINGS WITH GROUND EFFECT

Anmar H. Ali
Asst. Lect.
Univ. of Baghdad, College of Eng., Mech. Eng. Dept.

ABSTRACT

A numerical method for the calculation of the three-dimensional wake rollup behind symmetric wings with ground effect and its aerodynamic characteristics for steady low subsonic flow have been developed. A non-planar quadrilateral vortex-ring method with vortex wake relaxation iterative scheme for lifting surfaces is obtained. A computer program was build to treat wings with breaks, span wise trailing edge flaps, local dihedral angle, camber, twist and ground effect. Forces and moments are obtained from vector product of local velocity and vortex strength multiplied by density. The program has been validated for a number of configurations for which experimental data is available. Good agreement has been obtained for these configurations. Also many results obtained for different cases of wing with different shapes parameters.

الخلاصة

تم تطوير طريقة عددية لحساب دوران الاعقاب الهوائية الثلاثية الابعاد خلف الاجنحة المتماثلة مع التاثير الارضي عليها وخواصها الهوائية للجريان المستقر دون الصوتي. استخدمت الحلقات-الدوامية الرباعية الشكل غير المستوية مع طريقة التكرار المرن لدوامات الاعقاب الهوائية خلف اسطح الرفع. تم بناء برنامج حاسوبي ليتعامل مع الاجنحة ذات الكسرات، جنيحات عند الحافة الخلفية للجناح، زوايا ميلان محلية، تقوس، برم بالاضافة الى التاثير الارضي لها. تم ايجاد القوى والعزوم من الضرب الاتجاهي للسرعة المحلية وقوة الدوامة مضروبة بكثافة الهواء. اختبر البرنامج للعمل على عدد من الاشكال التي تتوافر البيانات العملية لها. اظهر البرنامج تطابق جيد لهذه الاشكال. كذلك ايجاد النتائج للعديد من متغيرات الاشكال المختلفة للاجنحة.

Keyword: potential flow, lifting surfaces, vortex lattice, wake roll-up, free wake model

INTRODUCTION

During the crucial phases of vertical take-off, hovering, and low-speed forward flight, the aircraft operate in a flow field which is significantly affected by the wake of the wing. The predominant feature of this wake is the presence of strong vortices shed from the blade tips, which then take an approximately helical trajectory, skewed by the motion of the craft. The close proximity of these vortices to one another and to the rotor blades can significantly modify the performance of the vehicle.

For high Reynolds Number flow past a thin wing at moderate angle of attack, convection dominates diffusion and the vorticity is confined to a thin, free shear layer. Under the influence of self-induced velocity, the shear layer has the tendency to rollup into the vortex cores. In the downstream direction, the vorticity is continuously fed into the vortex cores resulting in growth both in strength and dimension. At the stage where the vorticity contained within the cores, the velocity gradients are large and the viscous effect becomes important. So that, the present research only considers the initial stage of the wake rollup – potential flow - is considered with embedded vortex sheet.

The basic method is essentially an extension of the vortex lattice method, where the vortex sheet replaces the lifting surface and wake in classical theory is presented by distribution of quadrilateral vortex-ring which is solved to find the vortex strengths for the first calculation using the assumption of a stream wise wake from the actual trailing edge. In relaxing a vortex the calculation starts at the trailing edge and proceeds along the vortex in small straight line segments. The direction of each segment is being determined by the local velocity vector. This vector represents the stream velocity and the total induced velocity from surface and wake vortices including their reflections. By **[Butter and Hancock, 1971]** the wing is replaced by a lifting line bound vortex and the trailing vortex sheet is approximated by a number of discrete line vortices, the deformation of the trailing vortex sheet is determined. Further work to improve accuracy and understanding is required especially the accuracy in replacing a vortex sheet by a number of discrete vortices and improvement in the treatment of the tip region. **[Maskew, 1973]** examines the theoretical influence of camber and non-planar wake on the chance of lift, vortex drag and center of pressure of a rectangular wing with ground effect. Calculation are performed for two and three-dimensional potential flow for ground effect conditions. A quadrilateral vortex is used and reasonable accurate results are obtained. Many of the studies then use time dependent analogy to study the wake rollup for large aspect ratio cases. **[Katz, 1979]** illustrate the solution which is based on the time-stepping technique; where at the beginning of the motion only the wing bound vortices exist and the closing element of the trailing edge will be represent the starting vortex. At each time step, the wing is moved along its flight path and the trailing edge sheds a wake panel -vortex panel- with vortex strength equal to its circulation in the previous time step. This time-stepping methodology can then be contained for any type of flight path and at each time step the vortex wake corner points can be moved by the local velocity, so that wake rollup can be simulated. **[Johnson, et al., 1980]** improved panel method for the solution of three dimensional flows about wing and wing-body combinations with leading edge vortex separation are presented. The method employs a three-dimensional inviscid flow model in which the configuration, the rolled-up vortex sheets, and the wake are represented by quadratic doublet and linear source distributions. The strength of the singularity distribution as well as shape and position of the vortex spirals are computed in an iterative fashion starting with assumed initial sheet geometry. **[Yeh and Plotkin , 1984]** used higher-order panel method (Linear Vortex) to calculate the three-dimensional wake roll-up behind a large aspect ratio symmetric wings in steady inviscid incompressible flow. The wing span wise circulation distribution is obtained from lifting-line theory, and the wake geometry is then evaluated in an iterative fashion by satisfying conservation of circulation, flow tangency, zero pressure jumps for all wake panel surfaces. The method of time dependent analogy is used again to find the unsteady non-linear lateral subsonic characteristics of Delta wings with leading-edge separation by **[Katz, 1984]. [Gordon and Rom, 1985]** presented the flow over delta-shaped wing plan forms at high angle of attack in subsonic flow. A developed computational procedure to relax the wake is used where a finite number of line vortices used to represent the trailing vortex sheet. The wake geometry is evaluated in an iterative fashion starting from an assumed initial wake position. Good agreements are obtained with experimental results. **[Kroo and Smith, 1991]** presents a classical calculation of inviscid drag, based on far-field flow properties, is re-examined with particular attention to the non-linear effects of wake roll-up. This research included many of classical, linear results are more general than might have been expected. Wake deformation has been a little effect on

the induced drag of a single element wing. Far field trefftz-plane analysis may be used to estimate the induced drag of lifting systems. Also vortex model for wind turbine loads by **[Montgomerie, 2004]** was presented to evaluate the performance of the rotor blade of wind turbine. At last **[Bengin, 2005]** presented a numerical model for rotor blade loads calculation. The model was unsteady three-dimensional potential flow helicopter blade and the wake was allowed to freely convict along local velocity vector.

So that, the purpose of the present research to consider a low-order quadrilateral vortex-ring panel method for the vortex wake modeling including symmetry and ground effects. The technique is first developed for a finite wing in steady flight as the initial step towards the helicopter free-wake analysis or extension to non-linear effect of leading edge separation for low aspect ratio wings. It can be connected then with body and tail system to predict the non-linear characteristics on the wing-body-tail configurations.

MATHEMATICAL FORMULATION

A wing configuration is positioned at an angle of attack α in a uniform flow field of an undistributed velocity vector U_∞. The flow field is assumed to be steady, incompressible, inviscid, and irrotational except for isolated vortices. The presence of the wing creates a disturbance velocity potential ø that is governed by the Laplace equation;

$$\nabla^2 \phi = 0 \tag{1}$$

and by the boundary conditions on the wing surface and at the infinity. On the solid surface the total velocity has to satisfy the tangency condition;

$$\frac{\partial \phi}{\partial n_s} + U_\infty . n_s = 0 \tag{2}$$

and the disturbance velocity has to vanish at infinity;

$$\nabla \phi \to 0 \quad as \quad |r| \to \infty \tag{3}$$

Several additional conditions have to be satisfied.

1) The vortex wake *w* shed from the trailing edge of the lifting surface are free stream surface, i.e., they are tangent to the total velocity at every point.

$$\frac{\partial \phi}{\partial n_w} + U_\infty . n_w = 0 \tag{4a}$$

and they cannot support a pressure jump;

$$\Delta C_p \Big|_w \tag{4b}$$

2) The aerodynamic load must satisfy a Kutta condition along the trailing edge of the lifting surface that shed the separated vortices. This means a pressure jump across the trailing edge of the wing cannot be exists.

Eq. (1) and its boundary conditions constitute a mathematical formulation for the velocity potential ø. In spite of the Laplace equation being linear, the problem itself is non-linear because of the unknown spatial trajectories of the free vortices. These have to be determined as a part of the solution by the supplementary conditions as in **eq. (4)**, thus the problem defined non-linear.

According to Green's theorem, any function ø that satisfies the integral equation;

$$\phi(x,y,z)=\frac{1}{4\pi}\iint_{B}\left[\phi\frac{\partial}{\partial n}\left(\frac{1}{r}\right)-\left(\frac{1}{r}\right)\frac{\partial\phi}{\partial n}\right] \tag{5}$$

is a solution to **eq. (1)**, where ø is the disturbance potential at a point (x, y, z) in the flow field and r is the distance from this point to a point on the integration surface B that encloses all the singularities in the flow field. The disturbance velocity potential of a specific wing configuration can be calculated from a distribution on the surface B dipoles of intensities $\frac{\partial \phi}{\partial n}$ and ø that satisfies **eq. (5)** and boundary condition such as **eq. (2)** to **(4).**

In the present case, the lifting surfaces, on the other hand, are described by a distribution of bound vortices that is equivalent to the appropriate dipole distribution and that describes the tangential velocity and potential jump across the wing. Sources are not needed for the wing since their thickness is neglected. The trailing part of the bound vortices simulates the vortex sheets shed by the wing. Since the free-vortex lines follow stream lines, according to the Helmholtz theorems, **eq. (4)** can be replaced by the stream line equations

$$\frac{dy}{dx}=\frac{v}{U_\infty+u},\quad \frac{dz}{dx}=\frac{w}{U_\infty+u} \tag{6}$$

Eq. (1) and **(5)** are identically satisfied by the chosen distribution of singularities. The intensities of the singular elements and the trajectories of the free trailing vortices are determined by a simultaneous solution of **eq. (2)** and **(6).** This represents the mathematically non-linear problem of the wing and wake solutions that is solved by an iterative procedure.

METHOD OF SOLUTION

The lifting surface and its shed vortex wake are simulated by quadrilateral non-planar vortex-ring method. The main advantage of this method is in simple programming effort that it requires. Additionally, the exact boundary conditions will be satisfied on the actual wing surface, which can have camber, twist and various plan form shapes.

The method by which the thin-wing plane form and its shed wake are divided into panels as shown in **Fig. (1a)** and some typical panel elements are shown in **Fig. (1b)**. The leading edge of the vortex-ring is placed at the quarter chord line and the collocation point is at the center of three-quarter chord line at which the boundary condition is applied. The normal vector is defined at this point (control point). Free vortices are shed from the trailing edge of the wing; these vortices have strengths equal to the trailing edge vortices and Kutta condition satisfied automatically in this way,

$$\gamma_w=\gamma_{TE} \tag{7}$$

So that, its influence coefficients will be added to the trailing edge influence. An initial guess of the special trajectories of the free vortices is required to start the solution process. Wake panels, leaving the wing trailing edge at some angle above the wing surface (e.g., 1/2 α), are usually used **[Rusak et al., 1983]**. With the wake form predetermined, a simultaneous satisfaction of the tangency boundary condition **eq. (2)**

at all control point's results the following system of linear algebraic equations for the unknown intensities of the vortices;

$$\sum_{n=1}^{n_t} h_{kn}\Gamma_n + b_k = 0 \qquad (8)$$

where $(b_k = U_\infty \cdot n_s)_k$ is component of the free stream velocity in the direction normal to panel or cell **k** at its control point, and $\mathbf{n_t}$ is the total number of elements on wing and wake. $\mathbf{h_{kn}}$ are the influence coefficients of vortex-ring **n**, respectively, on control point **k**. An influence coefficient is defined as the component, normal to panel **k** at its control point, of the velocity induced there by a singular potential element of unit strength at **n. eq. (8)** can be rewritten in a matrix form as;

$$[A]\Gamma + b = 0 \qquad (9)$$

Where **A** is the influence coefficients matrix, Γ is the vector of singularity intensities and **b** is the vector b_k.

The solution of **eq. (9)** determines the strengths of the vortex-ring elements, which are then used to compute the velocities induced on the free vortices. **Eq. (6)** is next integrated to determine the equilibrium trajectories of the force-free vortices in the wake. This is done using an Euler method that aligns vortex segments with the stream line direction. With the new wake shape determined **eq. (9)** is then solved again for the new intensities of the vortices, and the calculation cycle is reiterated. The solution is considered to be converged when the changing in the vortex intensities are stopped within a given tolerance.

Once the solution is converged, where the method of Orthogonalization is followed to solve for unknown vortex strengths, the load distribution on the wing is computed using **Kutta-Joukowsky** equation, where the aerodynamic force and moment coefficients are calculated.

$$F = V \times \Gamma ds \qquad (10)$$

where **V** is the total resultant velocity at the point under consideration. The lift and induced drag values are obtained by taking the scalar product of **F** with unit vector normal to the free stream directions respectively.

$$L = F \cdot l$$
$$D = F \cdot d \qquad (11)$$

where ***l*** and ***d*** are the unit vectors in the lift and induced drag direction. Total moment is given by;

$$M = F \times R \qquad (12)$$

Where **R** is the vector joining the moment reference point to the line of action of **F**. The total lift, induced drag and moment are obtained by summing up these values for individual panels on the wing surface.

NUMERICAL PROGRAMMING ASPECTS

The method of calculating the wake shape behind a wing is implemented using a computer program where the wake panels vortices have been relaxed by evaluate the total velocity at a points located at the center distance of the wake trailing edge panel as shown in **Fig. (2)**. The total velocities mean the free stream velocity and induced

velocities due to vortex-ring distributed on the wing and wake surfaces. These velocities firstly calculated at all points defining in **Fig. (2),** and by using **eq. (6)** the trailing sides of the wake vortex panel are then moved with the local velocities, it must be note that the wake geometry is divided in to two region, near region which represents the deformed region and its length is approximated with two times wing span length the other is far region extended from the end of near region to infinity, this type of discretization prevents the effect of starting vortex on the wing loads. The procedure of iteration is continued in relaxation till the wake stopped its shape change. The other iteration is used to calculate the vortices strengths for the new wake relaxed. The calculation of intensities finished within a given accuracy. **Fig. (3)** shows block diagram of the calculations procedure of the program. In the result obtained so far there has been found a little change in vortex wake shape and force and moment characteristics after two iterations **[Maskew, 1973]**. However, it is found also the final shape of the vortex wake is affected by the segment length used; only with small vanishingly segment length will this be corrected, but at considerable expense in computer time. However if too large a segment length is used and a complicated wake is being calculated then the wake can diverge after a few segment lengths downstream from the tailing edge. The segment length to distance between vortices ratio of the order of unity has been found satisfactory so far **[Maskew, 1973]**. A computer program to deal with camber, swept, dihedral, twist, flapped wings with ground effect are calculated. Unless some programming improvements are incorporated, this will drastically increase the time of computation. Some of the programming technique adopted in the current work is discussed below.

The influence coefficients of the wing surface are computed firstly and then stored to be used in the next iteration, so that it is not need to recalculate wing influences during wake relaxation. To prevent wake to be over relaxation an approximate shape with half angle of attack are used for beginning iteration this may decrease the time required for the final wake shape. No improvements are done to decrease the computations of ring-vortex influence coefficients especially for the neighboring panels where edge sides are same between them. The wake shape iteration is fixed with constant number to prevent over relaxation.

RESULTS AND DISCUSSION

At first the proposed algorithm must be verified by comparing its results with experimental data obtained from published works. Load distribution is shown in **Fig. (4)** for two swept back trailing edge flapped wing where flap deflection is $\delta_f = 10^o$ and compared with results obtained from vortex-ring method with wake roll-up iteration. Although this represents complex case due to flap edges and effects of viscosity but it is found that good results are obtained as compared between them. The other comparison is the convergence properties of the method for a rectangular wing of AR=8 at 10^o angle of attack shown in **Fig. (5)**, where the number of panels in the span wise direction is varied from NY=10-30 elements. It is found that the wake is converged after two iterations with a good results obtained for wake shape behind it. So this method could be applied for different cases studied.

Fig. (6) shows the parameters of the wing investigated in the present work. The geometric details of the present calculations are,

AR =4.0, Taper Ratio TR = 1.0, Flap Chord/c =0.25, Flap Span/b =0.5, h/c =0.6, Ψ=0., β=0.

Fig. (7) shows the wing with its control points and vortex point in vortex-ring method without wake geometry where a straight lines emanating from the trailing edge and extended with a half angle of attack to far region. The span load distribution along the span is illustrated in **Fig. (8)**, where the angle of attack is 10^o without ground effect (free in air). The number of division in chord wise direction is Nx=5 and in the span wise direction is Ny=10.The figure also illustrates the load distribution with ground effect at h/c=0.6. The ground effect shows increase in lift or circulation generated by the wing along the span.

Fig. (9) shows top and back view of wake shape generated behind wing with previous geometric parameters, wing tip vortex and roll-up behavior is clearly shown in the figures. The trailing vortex core located nearly wing tips tends to bring the flow behind wing out in the tip direction, same thing observed with ground effect but with great vortex strength generated at wing tips, physically this trailing vortex is generated due to transfer the flow from high pressure at the wing bottom surface to low pressure at upper surface in other word tip represent the end of lift vortex, so a concentrated vortex generated at this position becoming the trailing vortex. The computer flow visualization shows that the ground effect deforms the wake behind the wing more than that when flying in free air as shown in **Fig. (10)**. The division numbers are Nx =5, NY=10 and the wake division number in the stream wise direction is Nw =30.

Fig. (11) shows the load distribution along the wing span with zero angle of attack and $\delta_f = 10^o$ deflected flap. The figure shows two curves free and ground effect. The difference is clearly showed increasing lift due to effect of ground on it. **Fig. (12)** the computer flow visualization behind wing for the case in **Fig. (11)**; it is clear that there is a vortex generated at the tip edge of the flap which is located at the center of half wing. The vortex core tends to roll-up the flow at this position. This vortex increases the deformed wake when the ground effect is accounted as shown in **Fig. (13).** Same divisions are used for this case with previous one.

Another effect may be studied is the twisting angle and its effect on the wake flow of wing. **Fig. (14)** shows the load distribution on the span wise direction for wing with twist angle $\beta = -8^o$ and angle of attack is $\alpha = 5^o$, the other parameters is fixed in the beginning of this section. It's clear that the angle of attack decrease along wing span, maximum at root and minimum at tip, so that, the load distribution give the same behavior where maximum at root and reversing its direction at the tip position. This load distribution showed that the wake generated is not deformed like other discussed cases; there is no wake roll-up as shown in **Fig. (15)**. Because of the angle of attack changed from root to tip due to twist the vortices emanating from trailing edge are not in the same plane, so that, its effects on each other are not strong as illustrated previously. The ground effect increases the loads and deformed wake as in **Fig. (16)**. In most present aircrafts, wings are twisted to firstly insure a good load distribution along wing span and secondly to prevent its deformed wake effect on the tail.

Fig. (17) illustrates the loads due to dihedral angle and compared without dihedral, there is no large difference between them except at the wing root where the load decrease due to decreasing of angle of attack. The angle of attack is $\alpha = 5^o$ and dihedral angle is $\theta = 10^o$. The wake form behind wing is shown in **Fig. (18)** with different sides; no major differences except that the inclination of dihedral angle are found in behavior with **Fig. (9)** in which dihedral angle is not used. **Fig. (19)** illustrate the ground effect on wing with dihedral angle, it is clear that the wing root affected with ground more than that at tip and this is the purpose of dihedral The physical meaning of dihedral angle is that the up wash velocity decrease with increasing wing

dihedral angle and this cause decreasing in the angle of attack and then decreasing loads.

Swept back wing is calculated in **Fig. (20)** where leading edge angle is 45^o, comparison of loads between free and ground effect are presented in figure. Wake shape is shown in **Fig. (21)** in different sides, one of the most important notes that the wake shape at the root has a little down ward flow; it means the angle of attack will be less than that at tip edge of the wing which is results of span wise load distribution. Another part of **Fig. (22)** is the ground effect which increase effect of trailing vortices and its rollup behavior.

For taper wing **Fig. (23)** shows wing vortex-rings and its control points with vortex points, its leading edge angle is $\Psi = 14^o$ and taper ratio is TR=0.5. Also **Fig. (23)** compares lift in span wise direction between free and ground effect. One can see that loads decrease rapidly than when taper ratio TR=1.0, so that appear in the wake visualization specially when viewed from back as shown in **Fig. (24)**, wake has less down ward flow at tip position from root due to decreasing load rapidly in direction to tip. Comparison for ground effect shows the deformed wake in **Fig. (25)**.

CONCLUSION

An analysis of rectangular vortex-ring lifting surfaces has been developed to calculate the wake roll-up for steady flow past a wing with high and moderate aspect ratio. The present wake model bears no small perturbation assumptions, and all of the equations are solved numerically. The flow field considered here is incompressible and inviscid, and wake is made of rectangular elements for the near region and semi-infinite stream wise direction vortices for the far region.

Good comparisons are obtained between present method and those in the literature for the rolled up wake geometries. The method capability to model wing with crack, swept, dihedral and taper flapped wings with ground effect. Care must be taken when discredited wake to prevent error from over estimation, as a role the ratio of panel dimensions of the wake must not exceeded one. The vortex-ring method with wake relaxation iterative scheme is seen to be a potentially powerful tool for handling complicated flow interference problems of this type.

Finally, the recommendations are suggested for further study or expansion of the method.

1- Studying the leading edge separation by adding free vortices extending from edge of the wing with same procedure discussed in this work.

2- Use of higher order method to increase the performance of calculations to remove the restrictions on wing descretization.

REFERENCES

Bengin A., "Three-Dimensional Rotor Flow Caculation," FME Transaction, Vol. 33, no. 1, 2005, pp. 33-39.

Butter B. J., Hancock G. J., "A Numerical Method for Calculating the Trailing Vortex System Behined a Swept Wing at Low Speed," The Aeronautical Journal, vol. 75,pp. 564-568, 1971.

Rajeswari B., Dutt H. N. V., "Nonplanar Vortex Lattice Method for Analysis of Complex Multiple Lifting Surfaces**,**" NAL, TM AE 8606, 1986.

Yeh D. T., Plotkin A., "Vortex Panel Calculation of Wake Rollup Behind a Large Aspect Ratio Wing," AIAA Journal, Vol. 24, no. 9, pp. 1417-1423, 1986.

Johnson F. T., Lu P., Tinoco E. N., "An Improved Panel Method for the Solution of Three-Dimensional Leading-edge Vortex Flow, Volume I, Theory Document," NASA CR-3278, 1980.

Kroo I., Smith S., 1991, "The Computation of Induced Drag with Non-planar and Deformed Wakes," NASA NCC-683, 1991.

Katz J., "Method for Calculating Wing Loading During Maneuvering Flight Along a Three-Dimensional Curved Path," Journal of Aircraft, Vol. 16, Nov. 1979, pp. 739-741.

Katz J., "Lateral Aerodynamics of Delta Wings with Leading-Edge separation," AIAA Journal, Vol. 22, no. 3, pp. 323-328, 1984.

Montgomerie B., "Vortex Model for wind Turbine Loads and Performance Evaluation," Swedish Defence Research Agency, Aeronautics FFA, September 2004, ISRN FOI-R—1301—SE.

Maskew B., "On the Influence of Camber and Non-Planar Vortex Wake on Wing Characteristics in Ground Effect," Loughborough University of Technology, Report C.P. 1264, 1973.

Gordon R., Rom J., "Calculation of Non-Linear Characteristics of Wings with Thickness and Camber at High Incidence," AIAA Journal, Vol. 23, no. 6, pp. 817-825, 1985.

Rusak Z., Wasserstorm E., Seginer A., "Numerical Calculation of Nonlinear Aerodynamics of Wing-Body Configuration," AIAA Journal, Vol. 21, no. 7, 1983.

NOMENCLATURE

A	Influence Coefficient Matrix	
AR	Aspect Ratio	
B	Wing and Wake Surfaces	m^2
b_k	Right Hand Side of Matrix	
b	Wing Span Length	m
c	Chord Length	m
C_p	Pressure Coefficint	
D	Induced Drag Force	N
dx, dy, dz	Element Distance	m
h_{kn}	Influence Coefficient of Element n on k	
h	Distance from Ground	m
L	Lift Force	N
M	Moment	N.m
n	Normal Vector	
r	Distance Between Points	m
TR	Taper Ratio	
U_∞	Free Stream Velocity	m/s
u, v, w	Perturbation Velocities	m/s
Ψ	Swept Back Angle	deg
α	Angle of Attack	deg
θ	Dihedral Angle	deg
β	Twist Angle	deg
ϕ	Potential Velocity	m^2/s
Γ	Circulation Strength	m^2/s
γ	Vortex Strength	m/s

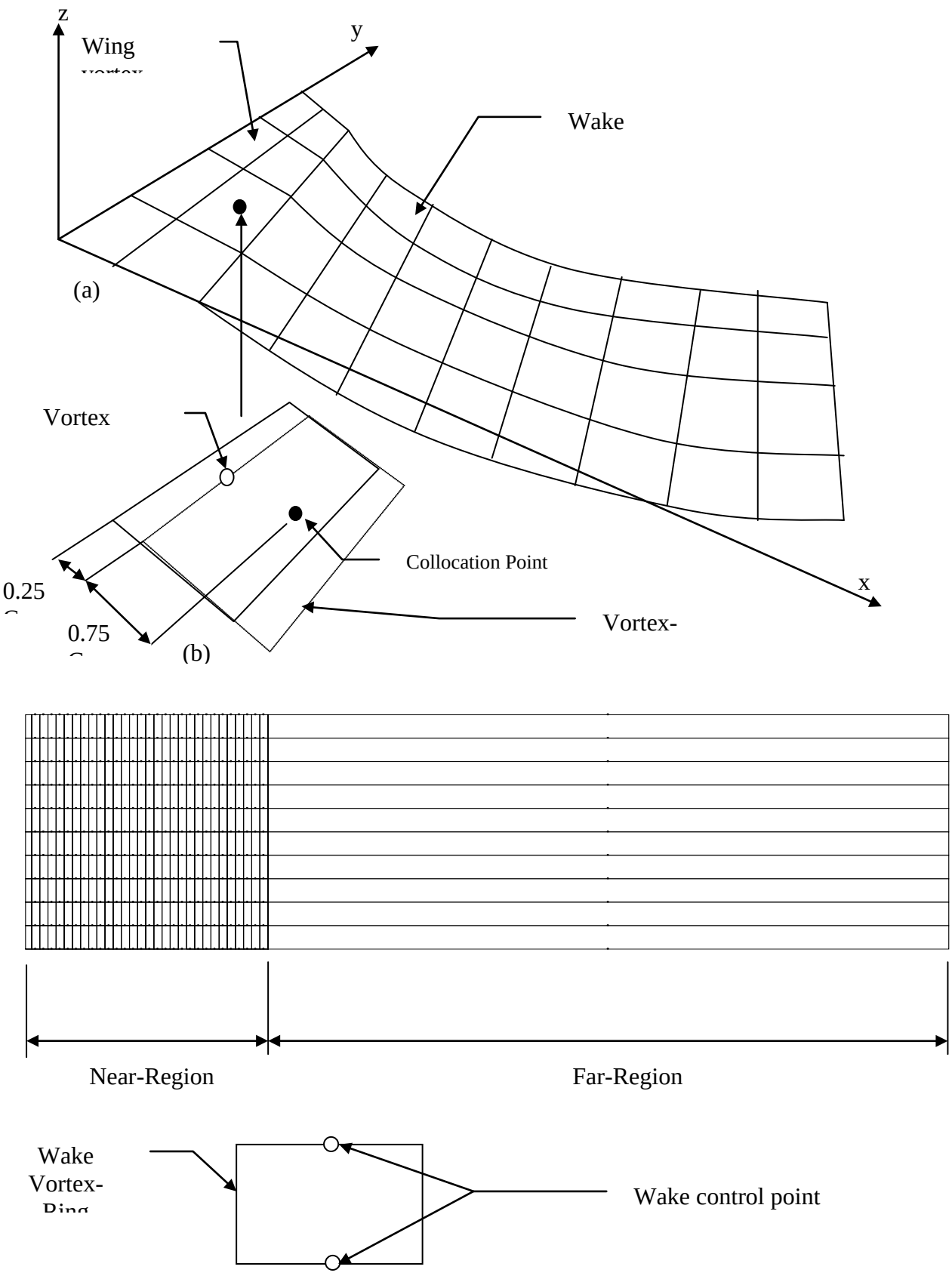

Fig. (2): Wake geometry and control points.

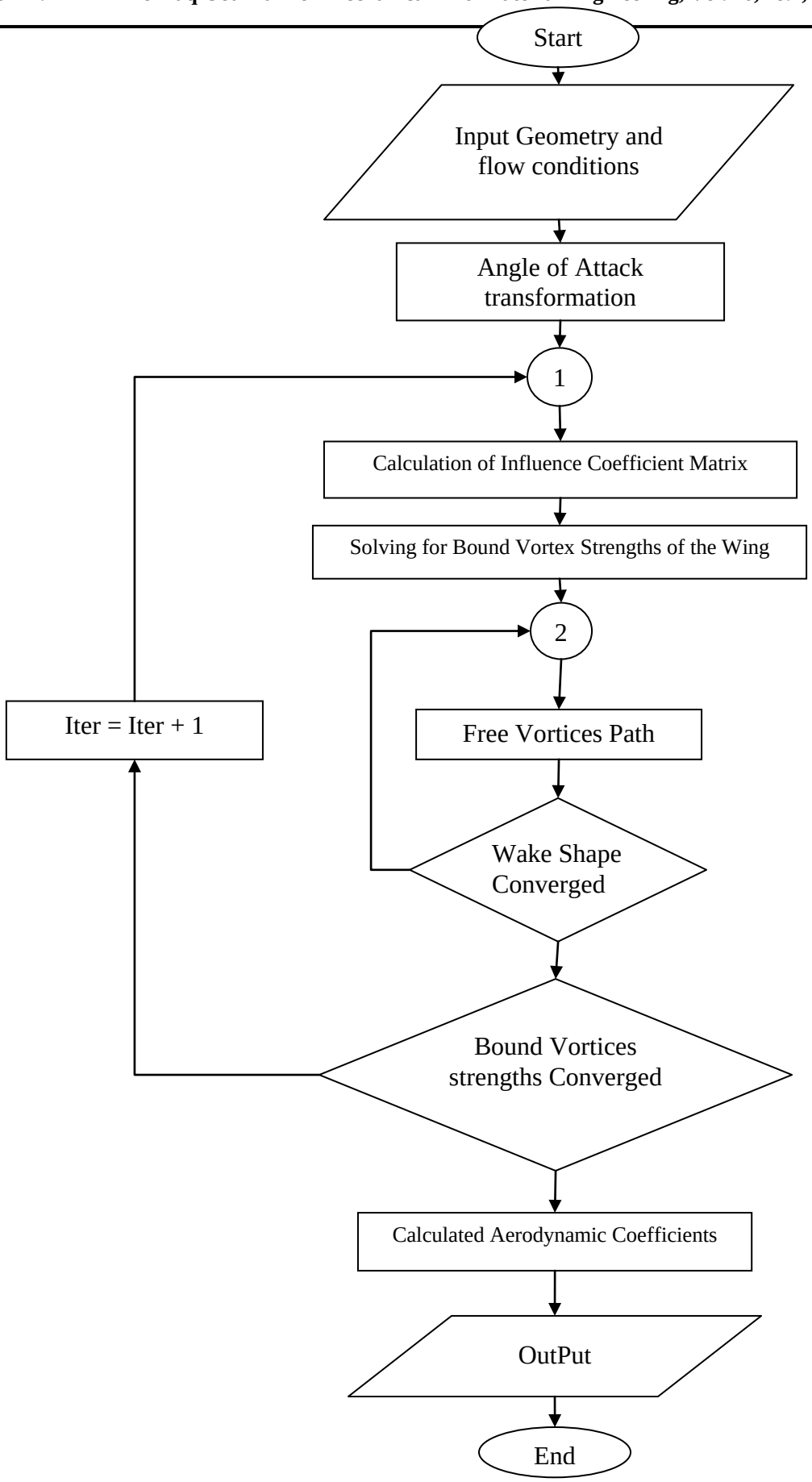

Fig. (3): Flow Chart Calculation Procedure of the Program.

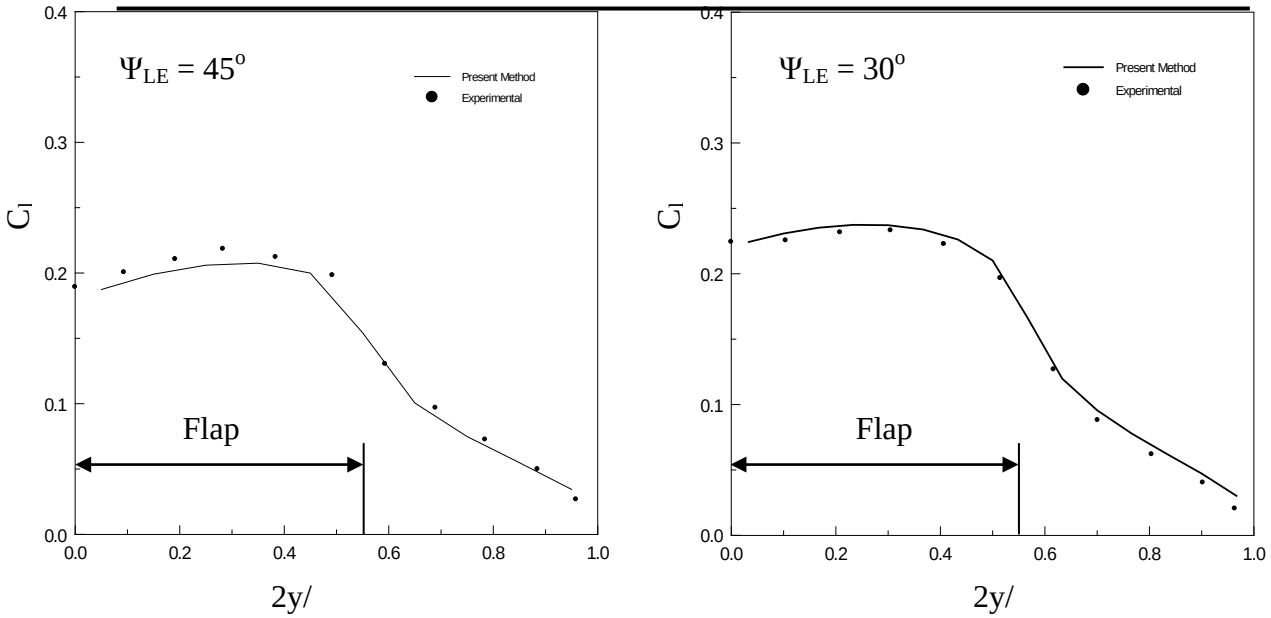

Fig. (4): Spanwise loading of swept back wings with inboard flaps, AR=4, $\alpha=0^o$, ($\alpha_f=10^o$, $c_f = 0.2c$, $y_f = 0.55$ b/2), Experimental from **[Rajeswari and Dutt,1986]**.

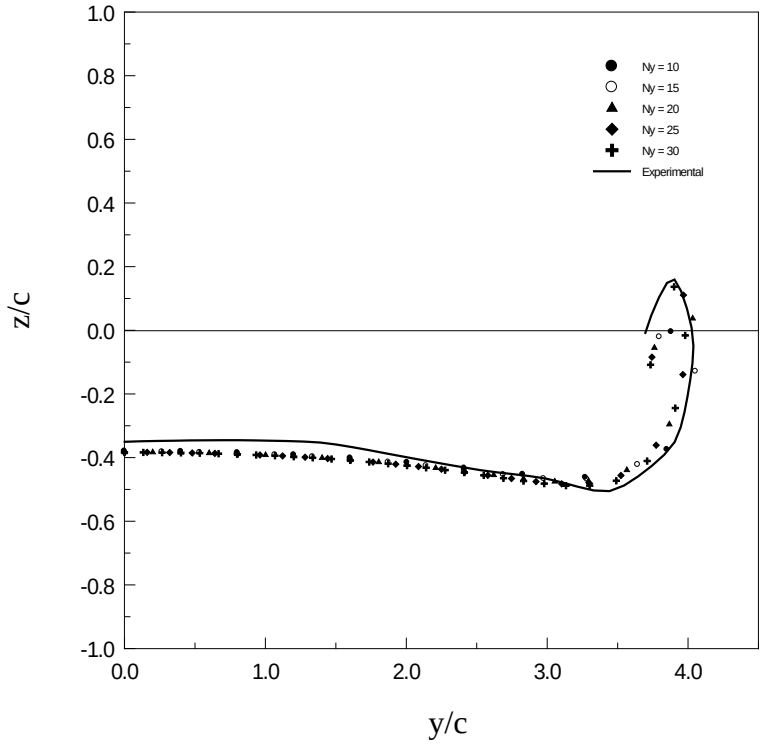

Fig. (5): Wake shapes at different angles of attack for rectangular wing: AR=8, $x_w/c=5$, Experimental from **[Yeh and Plotkin, 1984].**

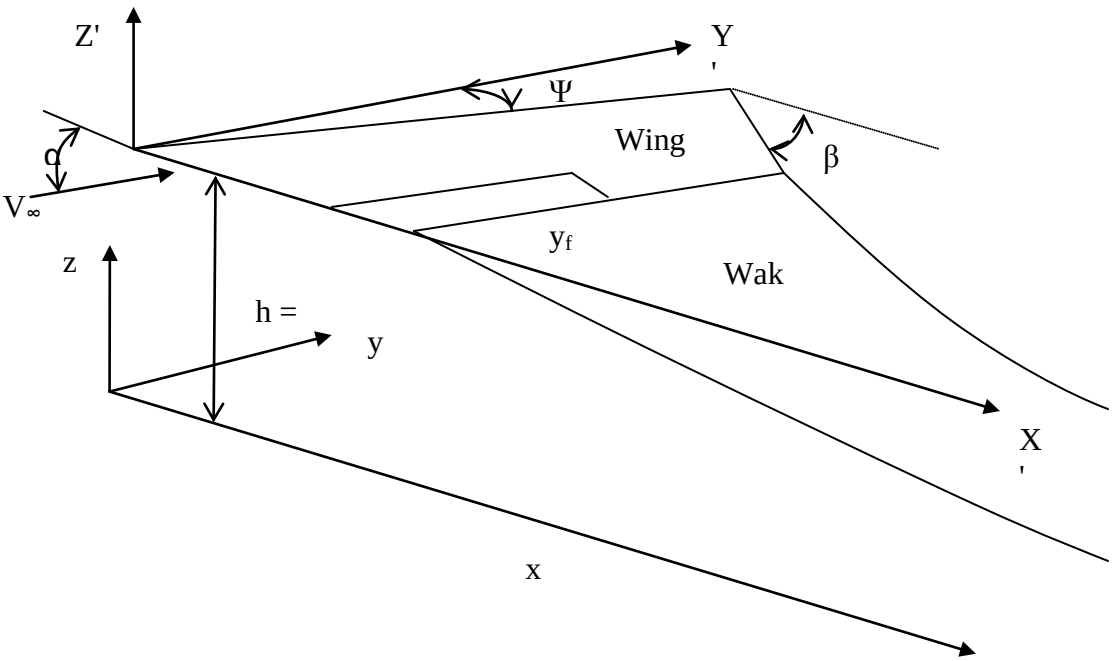

Fig. (6): Wing Shape Parameters.

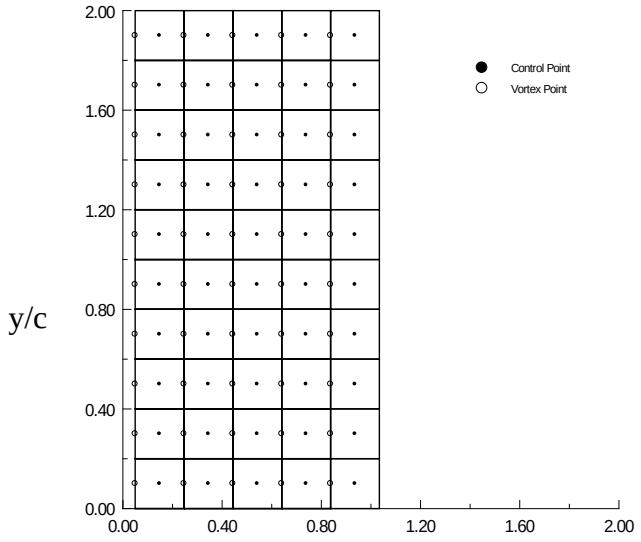

Fig. (7): Rectangular wing of AR=4 descretized with Vortex-Ring method.

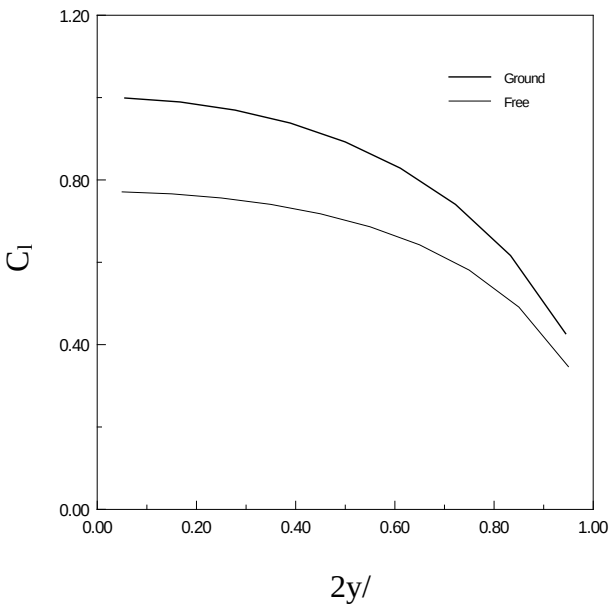

Fig. (8): Comparison between free flight and ground effect spanwise load of rectangular wing at $\alpha=10^{o}$.

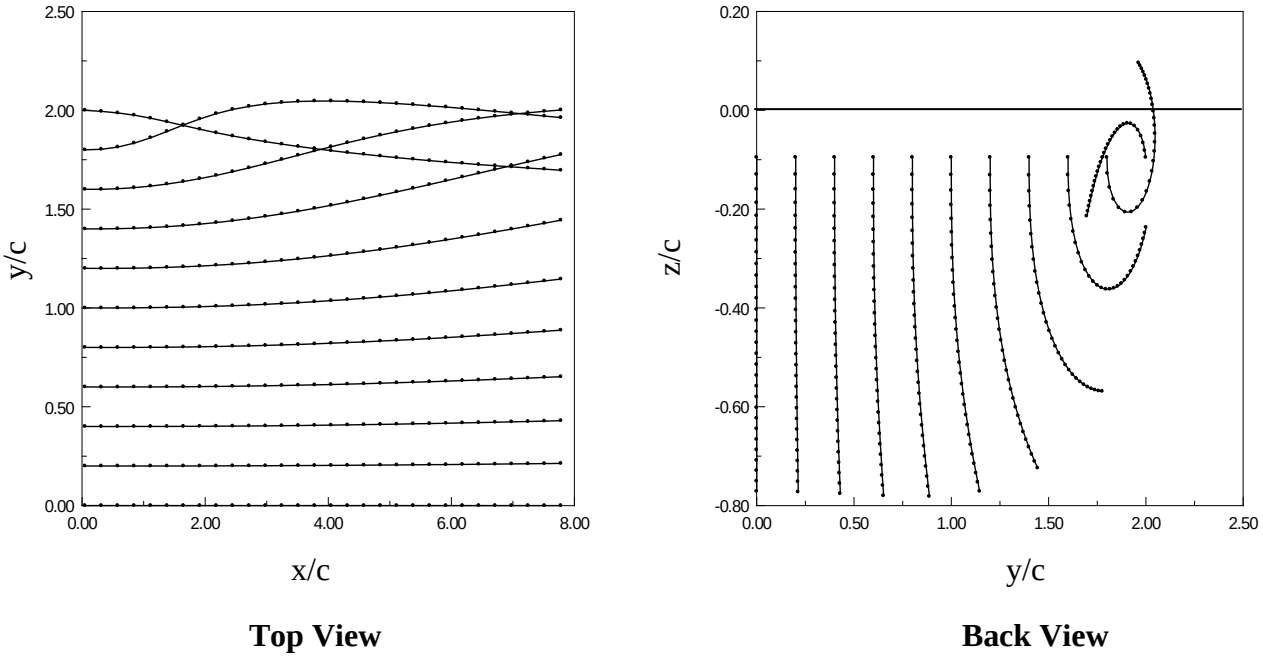

Top View **Back View**

Fig. (9): Projected Views of Wake just behind wing trailing edge of AR=4, α=10.

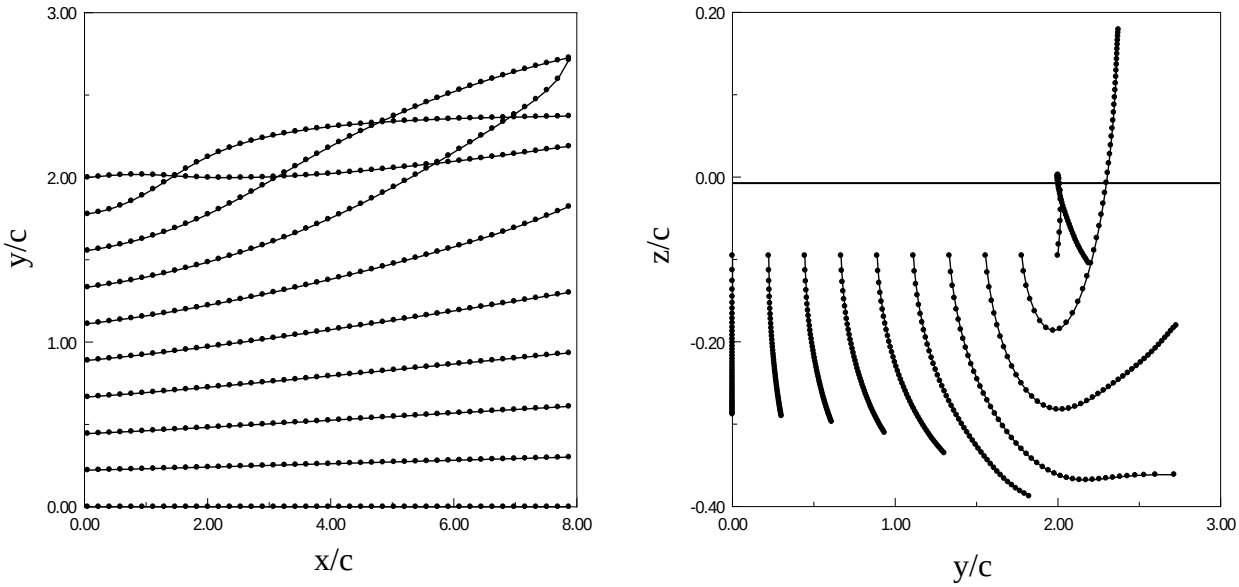

Top View **Back View**

Fig. (10): Projected Views of Wake with ground effect behind wing trailing edge of AR=4, α=10.

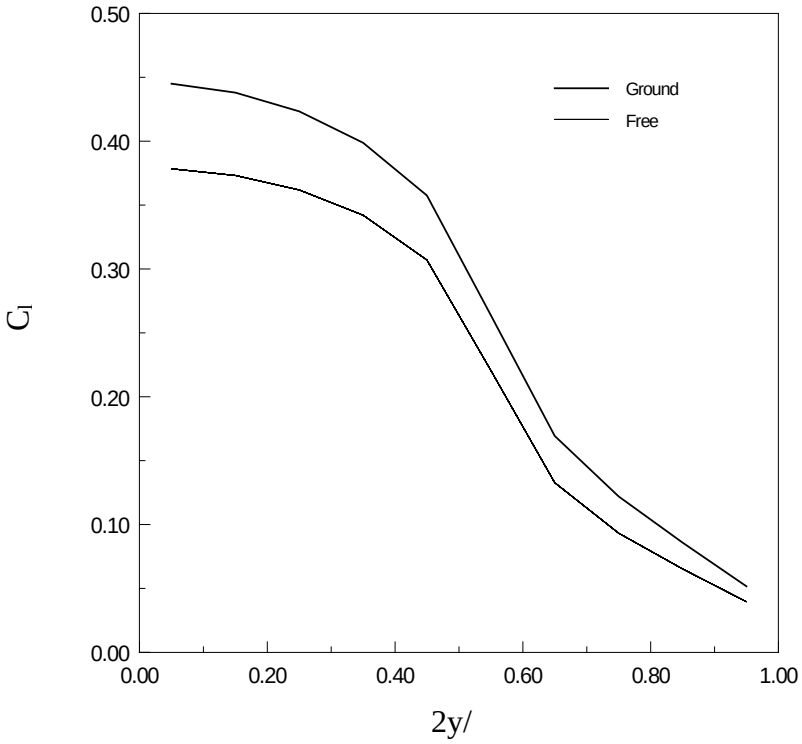

Fig. (11): Spanwise load distribution in Free and Ground effect of rectangular wing AR=4, Flap Deflection δ_f =10^o and α=0^o.

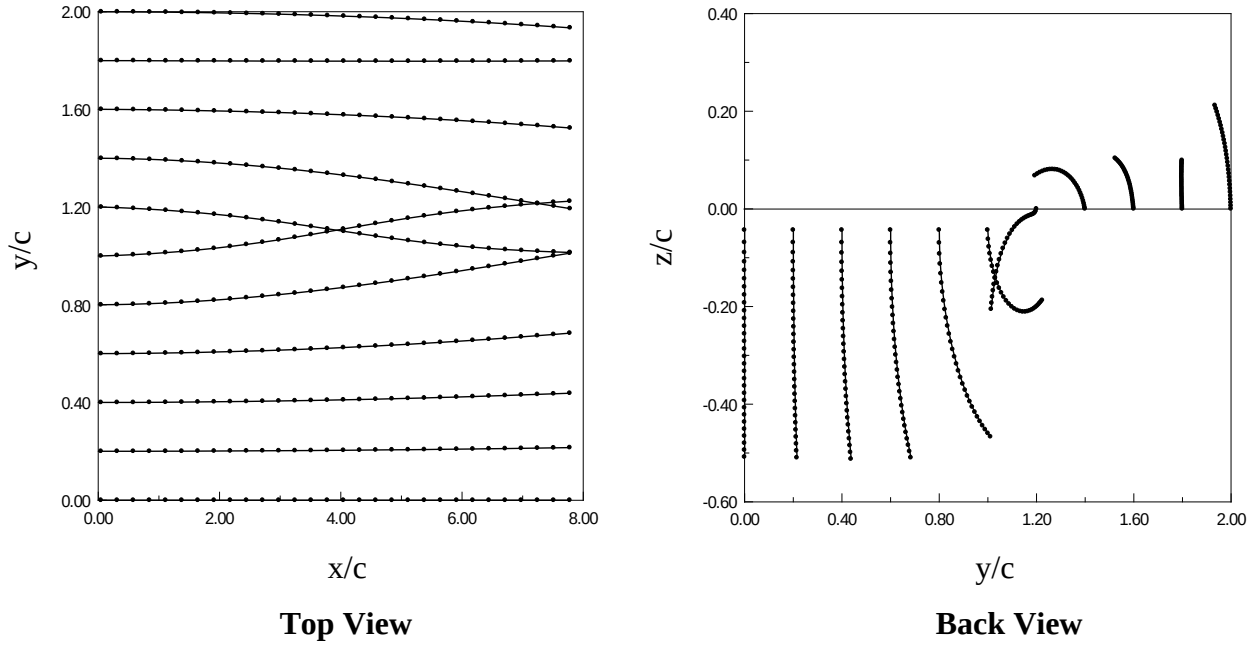

Fig. (12): Projected Views of Wake in Free air behind wing trailing edge of AR=4, α=0^o and δ_f=10.

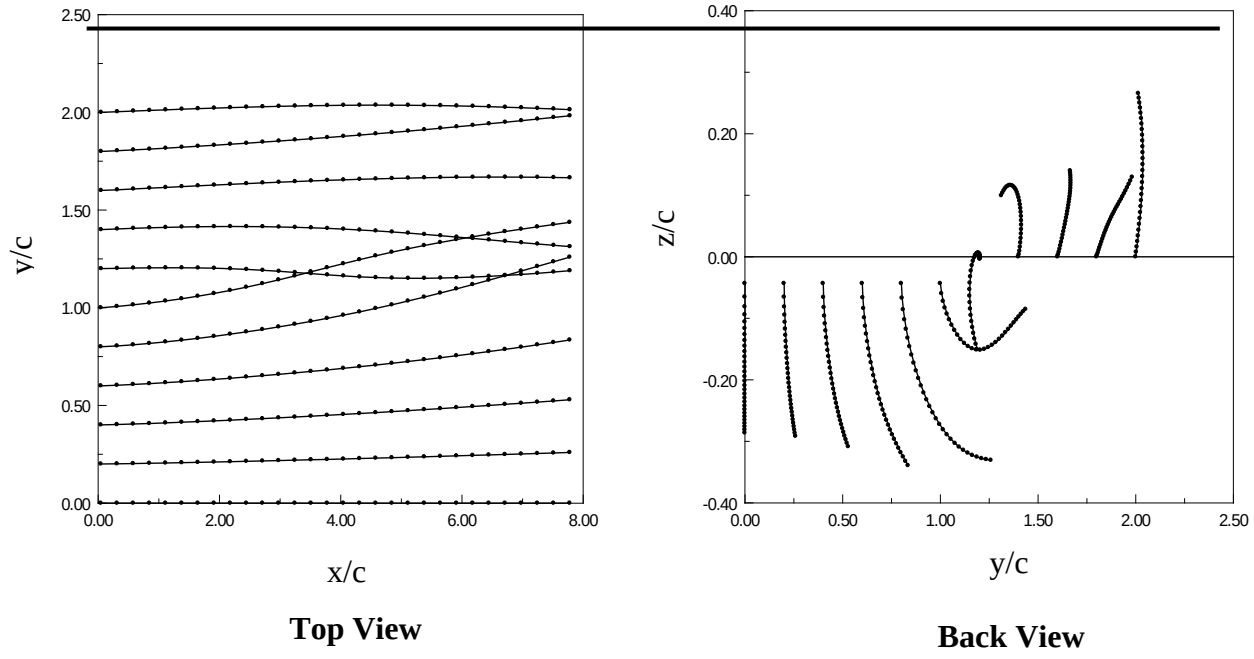

Fig. (13): Projected Views of Wake with Ground effect behind wing trailing edge of AR=4, $\alpha=0^o$ and $\delta_f=10$.

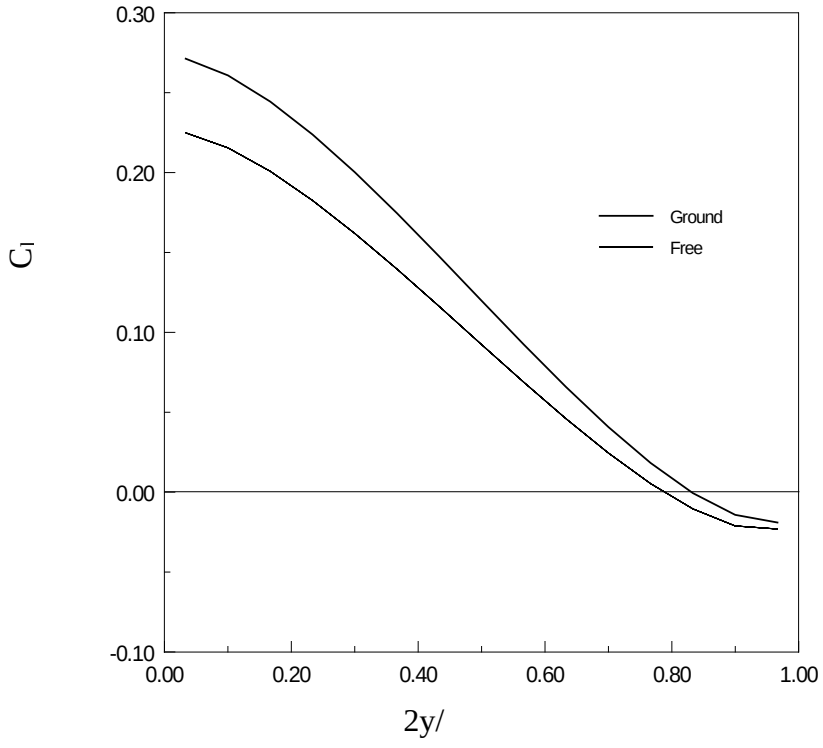

Fig. (14): Spanwise load distribution in Free and Ground effect of rectangular wing AR=4, Twist angle $\beta = -8^o$ and $\alpha=5^o$.

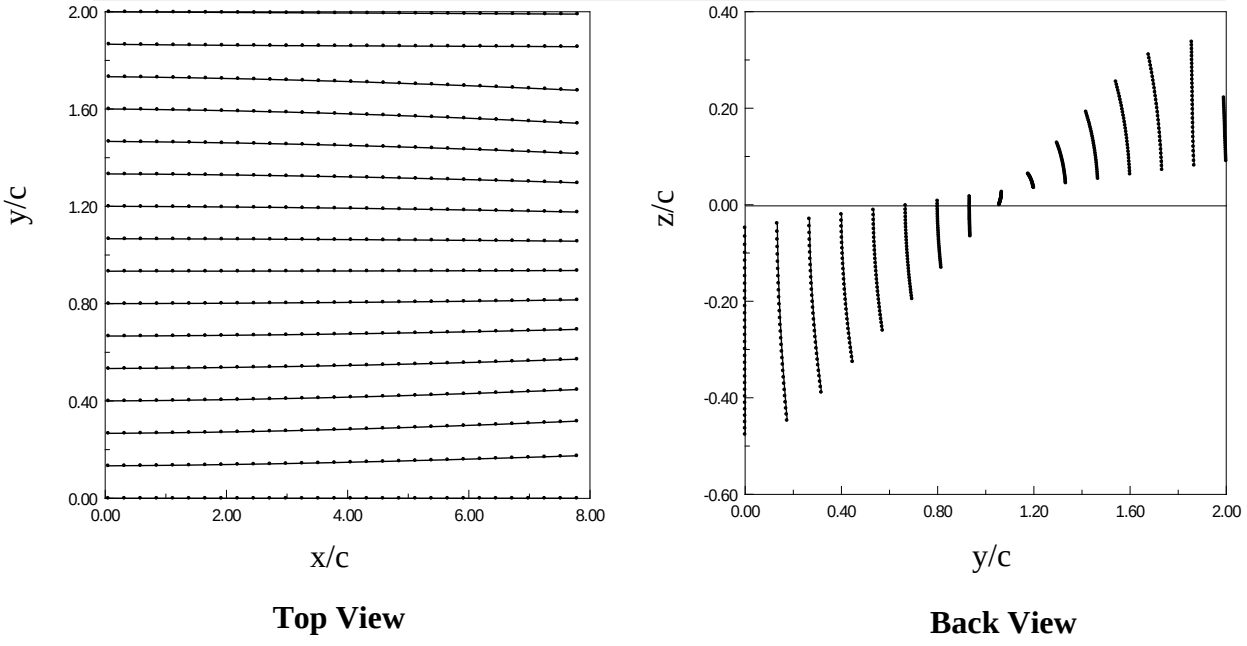

Fig. (15): Projected Views of Wake in Free air behind wing trailing edge of AR=4, $\alpha=5^{o}$ and Twist angle $\beta = -8^{o}$.

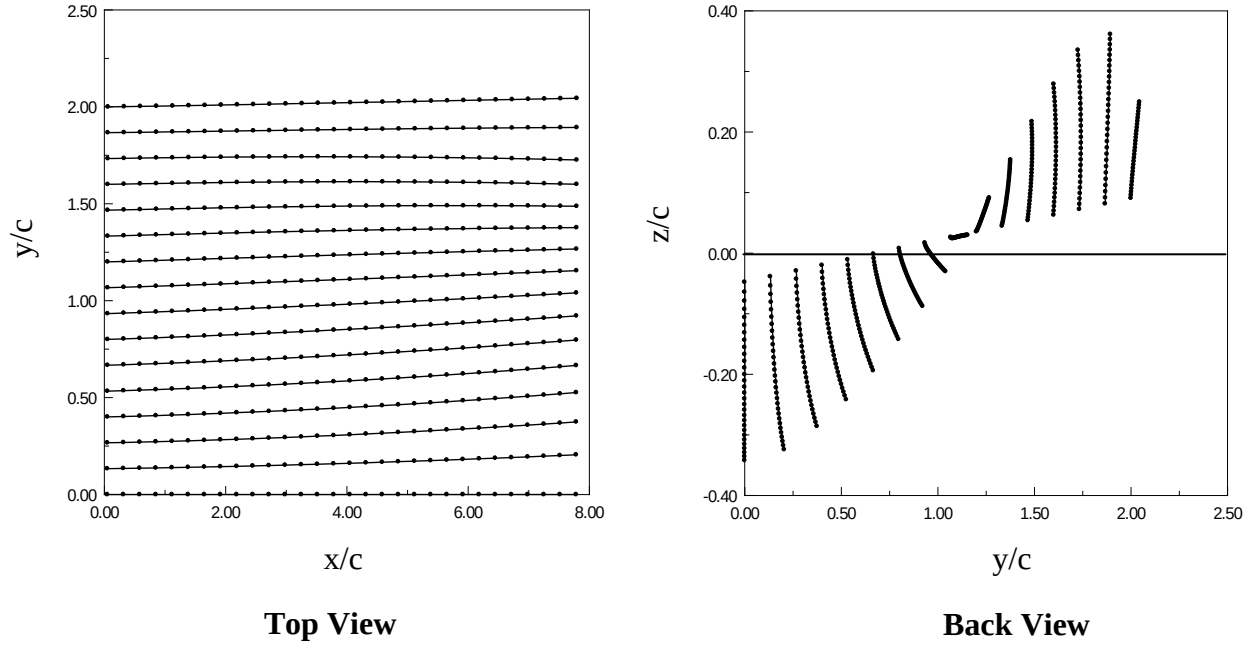

Fig. (16): Projected Views of Wake in Ground effect behind wing trailing edge of AR=4, $\alpha=5^{o}$ and Twist angle $\beta = -8^{o}$.

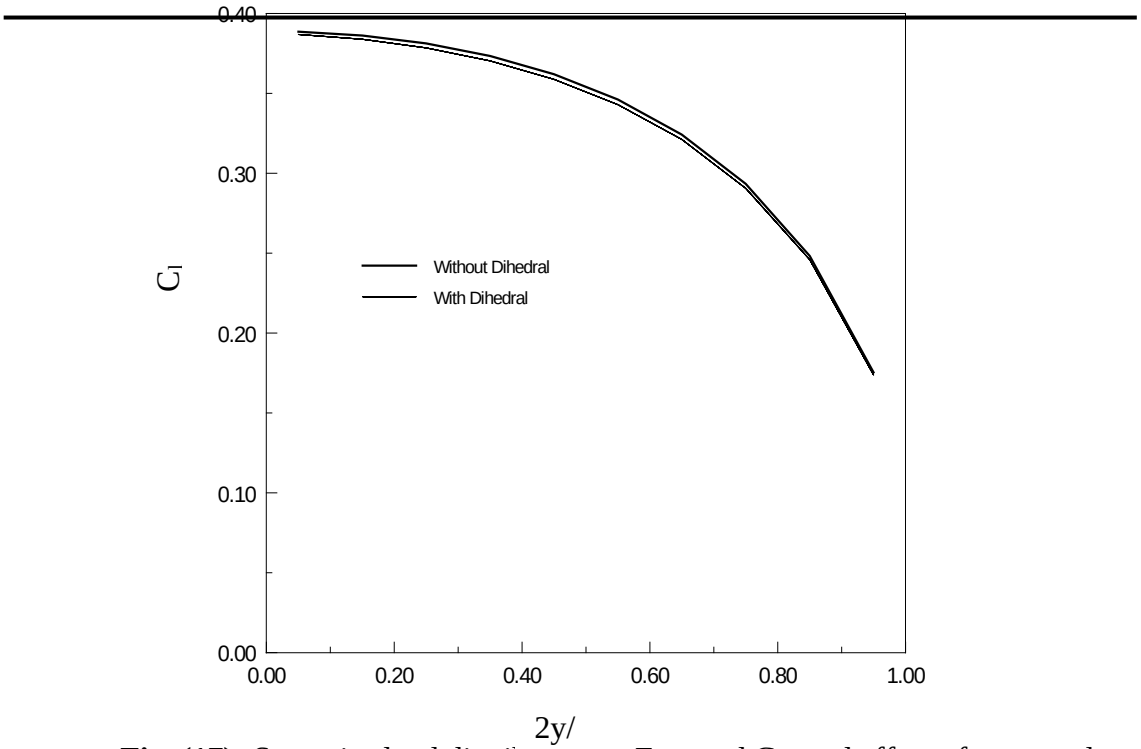

Fig. (17): Spanwise load distribution in Free and Ground effect of rectangular wing AR=4, Dihedral angle $\theta = 10^o$ and $\alpha=5^o$.

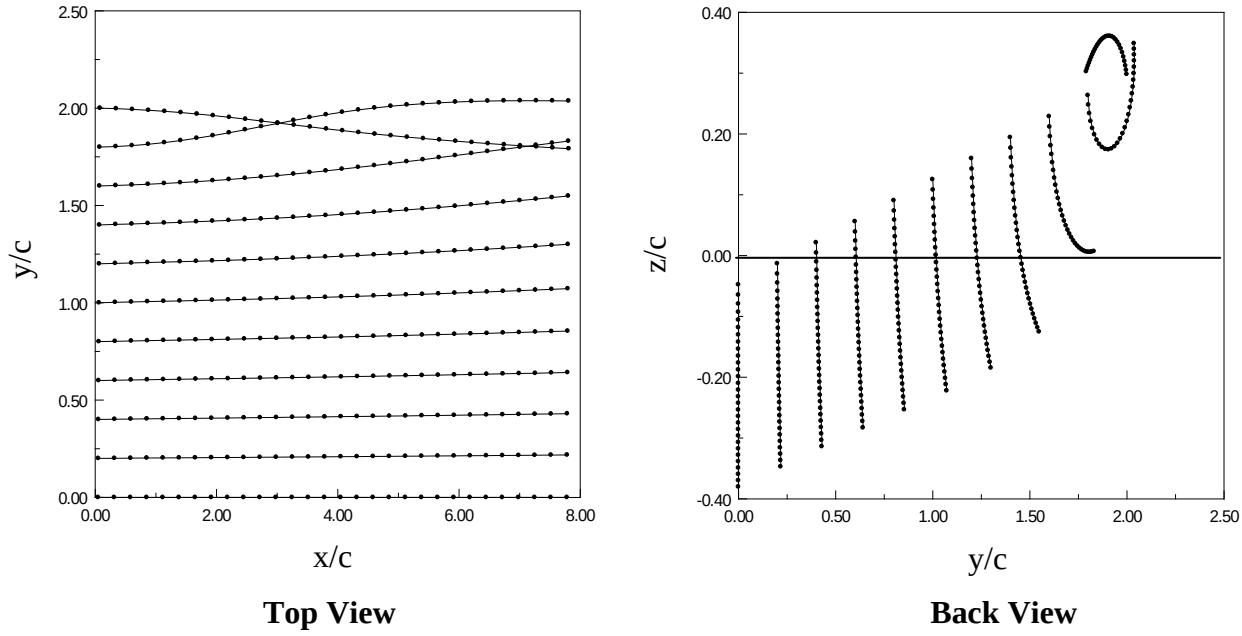

Fig. (18): Projected Views of Wake in free air behind wing trailing edge of AR=4, $\alpha=5^o$ and Dihedral angle $\theta = 10^o$.

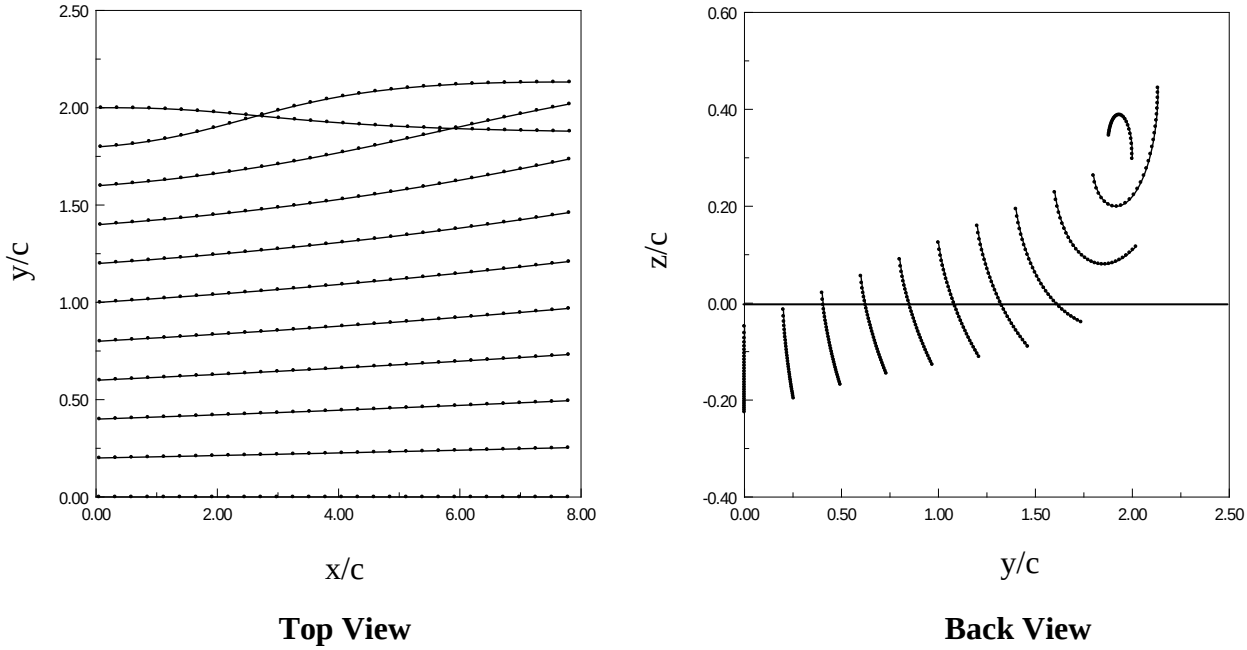

Fig. (19): Projected Views of Wake in Ground effect behind wing trailing edge of AR=4, $\alpha=5^o$ and Dihedral angle $\theta = 10^o$.

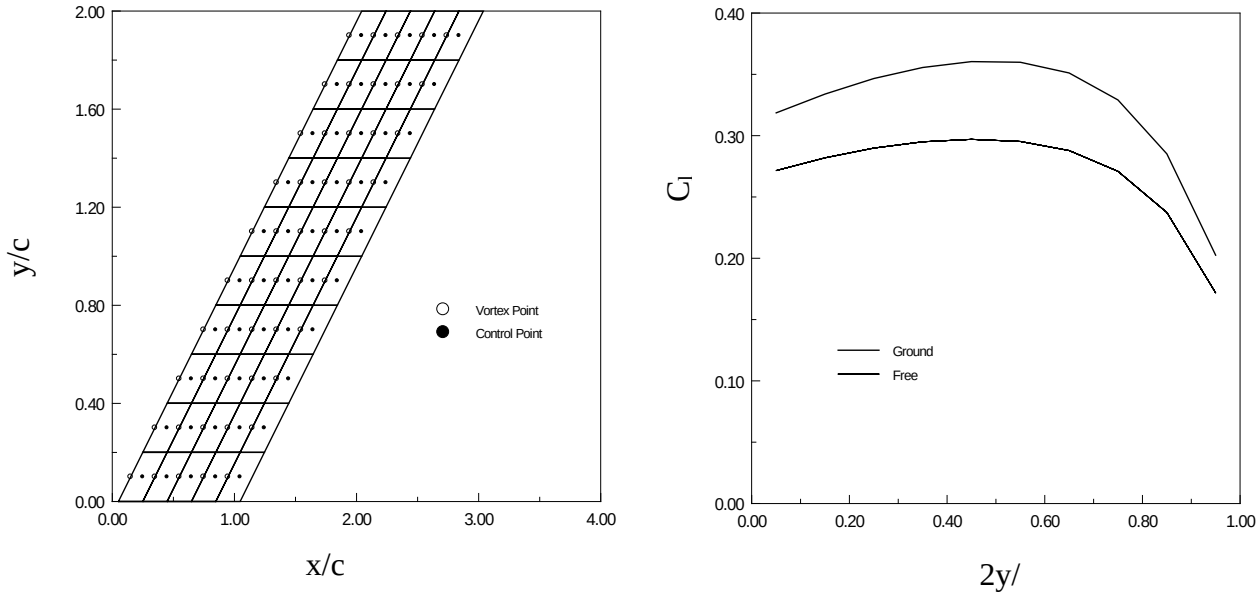

Fig. (20): Wing of AR=4, Swept back angle $\Psi = 45^o$ descretization and span wise load distribution with free and ground effect.

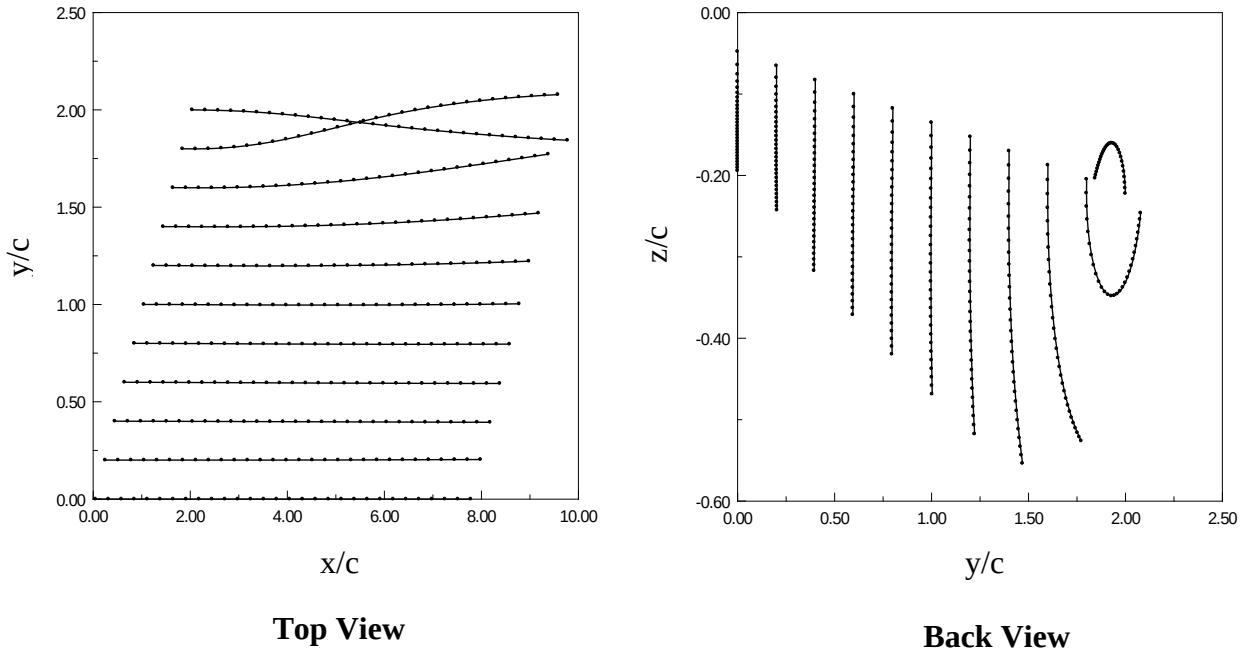

Top View **Back View**

Fig. (21): Projected Views of Wake in Ground effect behind wing trailing edge of AR=4, $\alpha=5^o$ and Swept angle $\Psi = 45^o$.

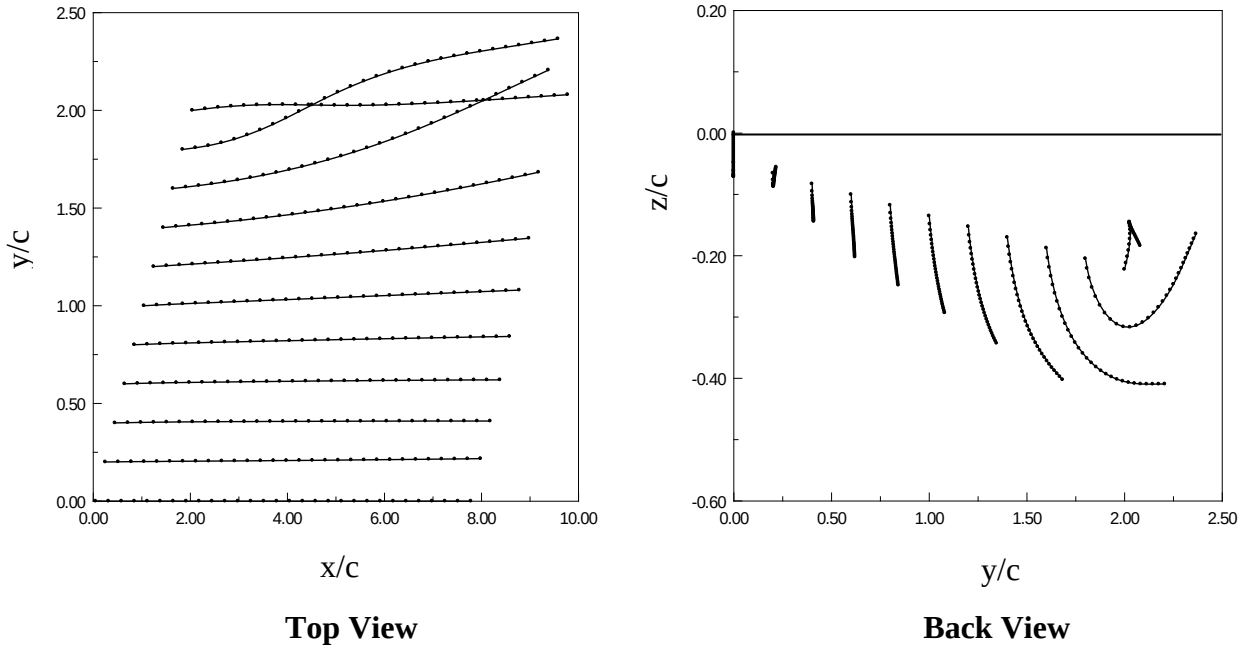

Top View **Back View**

Fig. (22): Projected Views of Wake in Ground effect behind wing trailing edge of AR=4, $\alpha=5^o$ and Swept angle $\Psi = 45^o$.

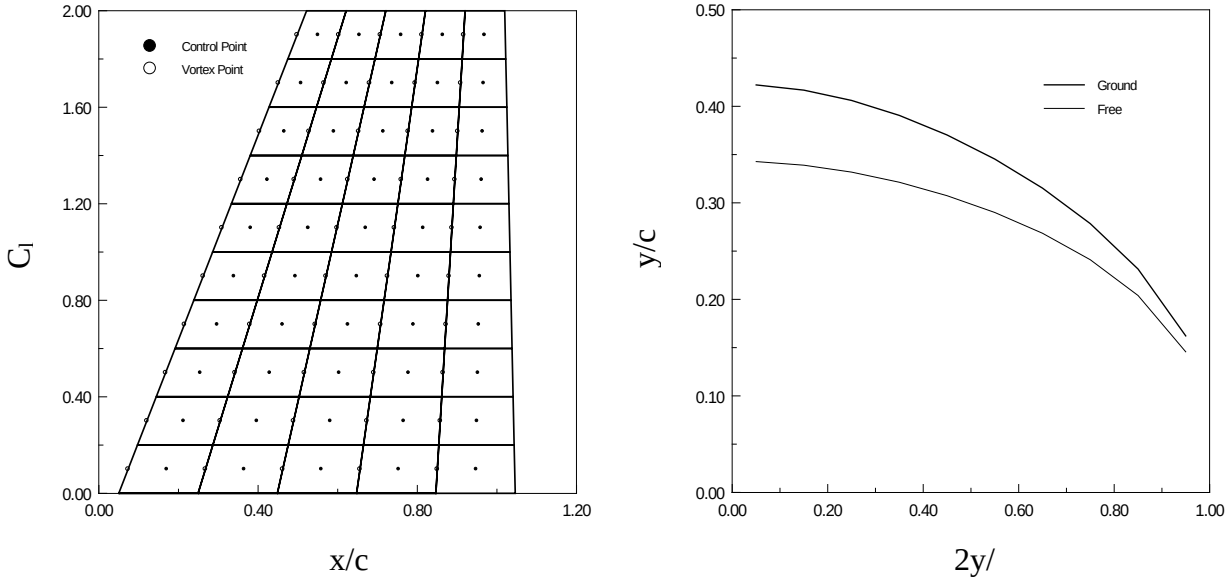

Fig. (23): Wing of AR=4, Swept back angle $\Psi = 14^{o}$ and Taper ratio TR= 0.5 descretization and load distribution with free and ground effect.

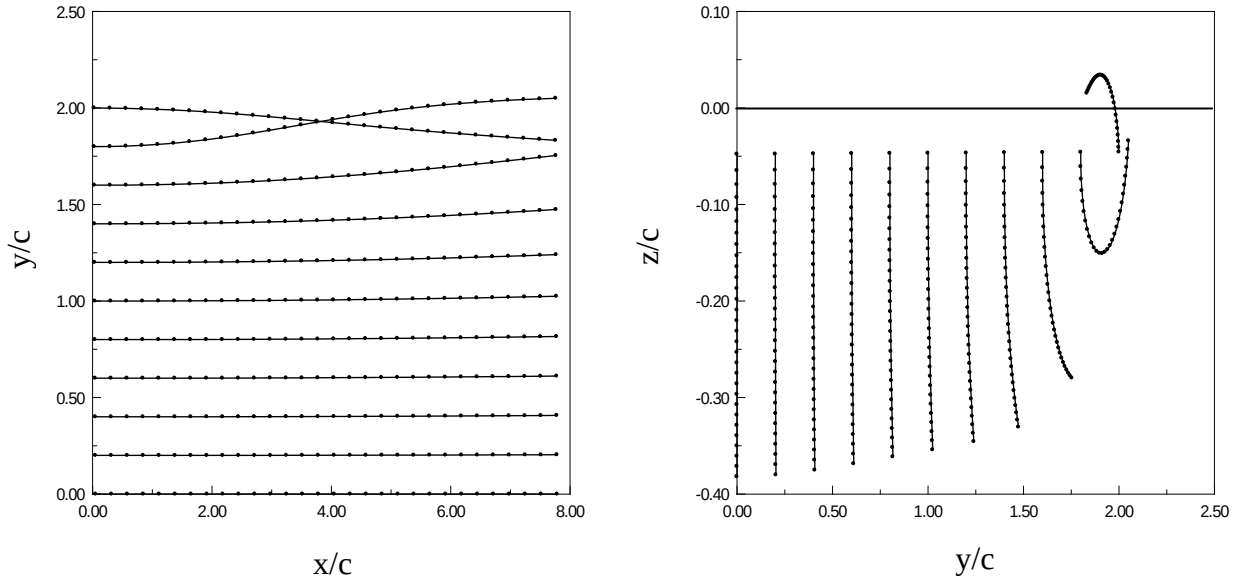

Top View **Back View**

Fig. (24): Projected Views of Wake in Free air behind wing trailing edge of AR=4, $\alpha = 5^{o}$, Swept angle $\Psi = 14^{o}$ and TR=0.5.

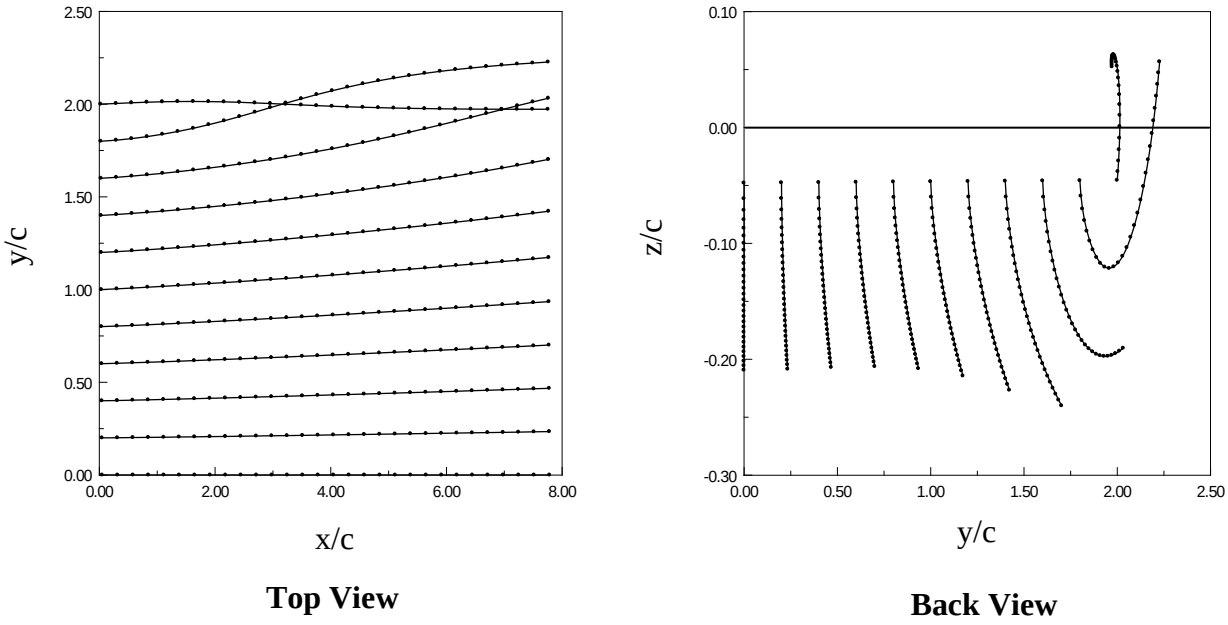

Fig. (25): Projected Views of Wake in Ground effect behind wing trailing edge of AR=4, $\alpha=5^{o}$, Swept angle $\Psi = 14^{o}$ and TR = 0.5.